IEEE Access
Multidisciplinary ⋮ Rapid Review ⋮ Open Access Journal

Received October 29, 2020, accepted November 17, 2020, date of publication November 25, 2020,
date of current version December 9, 2020.

Digital Object Identifier 10.1109/ACCESS.2020.3040558

Virtual-Vector-Based Model Predictive Current Control of Five-Phase PMSM With Stator Current and Concentrated Disturbance Observer

TIANXING LI[1], RUIQING MA[1], (Member, IEEE), AND WEIJIAN HAN[2], (Member, IEEE)
[1]School of Automation, Northwestern Polytechnical University, Xi'an 710072, China
[2]State Key Laboratory of Reliability and Intelligence of Electrical Equipment, Hebei University of Technology, Tianjin 300401, China

Corresponding author: Tianxing Li (litianxing@mail.nwpu.edu.cn)

ABSTRACT The finite control set model predictive current control(FCS-MPCC)can significantly improve the dynamic performance of the five-phase permanent magnet synchronous motor (5P-PMSM), but its control performance highly depends on the accuracy of the model parameters. The parameter error compensation based on the first-order sliding mode observer can improve the robustness of FCS-MPCC under Model parameter mismatch. The introduction of the sign function leads to chattering in the observation results. In order to eliminate this chattering, a first-order low-pass filter needs to be added for compensation. However, the introduction of filters will increase system design difficulty and bring system delays, which will affect the compensation effect. Therefore, a second-order sliding mode observer, based on the variable-gain Super-Twisting algorithm, is proposed to realize the parameter error estimation and one-beat delay compensation in this paper. By establishing the Lyapunov function, the stability proof of the proposed observer, and the calculation method of the observer parameters are given. Besides, the third harmonic current can be suppressed, and the computational burden of the control unit can be reduced by controlling the proportion of medium vector and large vector reasonably. According to the deadbeat control, the optimal virtual voltage vector action time in each cycle is obtained, which improves the tracking ability of the reference current. At last, Extensive experimental results validate that i) the proposed observer can significantly improve the robustness of model predictive current control even under parameters mismatch; ii) the proposed control method can effectively enhance the dynamic performance of the 5-phase PMSM.

INDEX TERMS Five-phase PMSM, finite control set model predictive current control (FCS-MPCC), duty ratio, virtual voltage vector (V3), variable-gain super-twisting algorithm (VG-STA).

I. INTRODUCTION

In the past decades, the concept of all-electric aircraft (or more electric aircraft) was proposed, resulting in the extensive use of electric driving systems on aircraft, such as electric brakes, spoilers, and fuel pumps. The ever increasing demand for electricity on large airplanes has set higher standards for power density, reliability, and safety. The five-phase PMSM stator comprises multiphase windings, showing higher reliability, power density, and fault tolerance than the three-phase PMSM (3P-PMSM).

At present, current control strategies of the 3P-PMSM are generally divided into Field Oriented Control (FOC), Direct Torque Control (DTC), and FCS-MPCC [1]–[3]. Compared with FOC, FCS-MPCC can obtain a better dynamic response. Compared with DTC, FCS-MPCC provides more flexible optimization methods thanks to its high control freedom, resulting in more accurate and effective optimal voltage vector optimization [1].

However, there are still some unsolved problems of FC-MPCC when applied to 5P-PMSM. Due to the stator-rotor air gap and stator winding distribution, the third harmonic current participates in the motor energy exchange of 5P-PMSM. Compared with three-phase PMSM, the prediction model and the constraints of 5P-PMSM for FC-MPCC are more complicated, with tripled base voltage vectors in the optimization process. The significantly increased calculation burden of FC-MPCC, when applied to

The associate editor coordinating the review of this manuscript and approving it for publication was Ning Sun.

5P-PMSM, may make the controller unable to complete the optimization process within one control period, resulting in poor control performance.

For multiphase motors, the non-zero switching state generates a voltage vector on both the α-β subspace and x-y subspace simultaneously. To suppress the third harmonic current and simplify the optimization process, a virtual voltage vector group, synthesized by two non-zero switching functions, is used for the FCS-MPCC of the six-phase motor [4]–[7]. These two non-zero switching functions generate two in-phase fundamental voltage vectors in the α-β subspace and two out-of-phase third harmonic voltage vector in the x-y subspace.

In addition to the computational burden, the control performance of FCS-MPCC is also highly dependent on the accuracy of the controlled object parameters. In order to reduce the effect of parameter mismatch on the performance of FCS-MPCC, online parameter identification strategies were proposed. At presented, online parameter identification strategies mainly includes model reference adaptation [8], [9], particle swarm optimization algorithm [10], genetic algorithm [11], immune algorithm [12], least-square method [13], Kalman filter [14] and observer-based identification algorithm. Shah *et al.* [15] compared the above seven parameter identification methods from convergence speed and computational cost. Among them, the observer-based identification algorithm is more robust while ensuring real-time performance.

Observer-based identification algorithms include disturbance observer [16]–[21] and sliding-mode observer (SMO). De Soricellis *et al.* [16] adopted a disturbance observer to replace the decoupling network of the current loop, which avoids the influence of the motor rated parameter mismatches and improves the robustness of the current loop. Zhang *et al.* [17] used a disturbance observer to observe the stator flux linkage to eliminate the disturbance error caused by the motor parameter mismatch of the prediction model. Except for the motor parameters, some uncertain factors in the modeling process can also affect the performance of FCS-MPCC control. The different disturbances are combined as a concentrated disturbance in the prediction model to simplify the analysis and facilitate the realization [18]–[22].

Sliding-mode observer, as a variable structure observer, insensitive to the variation of system parameters, shows a faster convergence rate and better robustness. It can realize the observation of parameter mismatch and uncertain factors in continuous linear systems [23]. Deadbeat Predictive Current Control (DPCC) is a current control strategy based on the motor model, whose control performance is also affected by modeling errors. Zhang *et al.* [24] proposed a DPCC with a first-order SMO for PMSM, which is used to observe the combined parameter disturbance in the prediction model and compensate for the d-p axis voltage output. However, due to the high-frequency switching function Sign $(*)$ used in the first-order sliding mode algorithm, the observed results showing a chattering phenomenon. However, first-order low-pass filters can attenuate the chattering, but not completely. A high-order sliding mode algorithm can alleviate the chattering by integrating the sign$(*)$ [25]–[28]. When the order of SMO is higher than two, a higher-order derivative operation will be introduced, which increases the calculation burden. The second-order SMO based on STA can avoid higher-order derivative operations [27], [28]. However, the STA algorithm includes a square root operation, which slows the convergence rate when sliding mode variables are far from the sliding mode surface. To solve this problem, Gonzalez *et al.* [29] proposed a VG-STA algorithm to improve the convergence speed of sliding mode variables in the whole process.

Considering the characteristics of 5P-PMSM, in this paper, we improved the traditional FCS-MPCC by enhancing its robustness to parameter perturbations. The structure of this paper is organized as follows. In Section II, a virtual voltage vector group based on large and medium voltage vectors is proposed to reduce the computational burden of FCS-MPCC. On this basis, a method to calculate the optimal voltage vector acting time based on deadbeat theory is proposed to improve the current waveform. In Section III, the influence of the motor parameter mismatches on the optimal voltage vector optimization process and the calculation of the optimal voltage vector action time is analyzed. In Section IV, to achieve robust current control, a second-order SMO based on the VG-STA algorithm is presented for parameter mismatch and one-beat delay compensation. In Section V, comprehensive experimental tests were performed to verify the proposed current control approach and the optimal action time of the voltage vector calculation method. Section VI concluded this paper.

II. FCS-MPCC OF 5F-PMSM

The static coordinate system used for Clark transformation of 5P-PMSM can be divided into two subspaces of α-β and x-y, corresponding to the fundamental harmonic mathematic model and the third harmonic mathematic model:

$$\begin{bmatrix} L_{m1}\dfrac{di_\alpha}{dt} \\ L_{m1}\dfrac{di_\beta}{dt} \\ L_{m3}\dfrac{di_x}{dt} \\ L_{m3}\dfrac{di_y}{dt} \end{bmatrix} = -R\begin{bmatrix} i_\alpha \\ i_\beta \\ i_x \\ i_y \end{bmatrix} + \begin{bmatrix} u_\alpha \\ u_\beta \\ u_x \\ u_y \end{bmatrix} - \omega_e \begin{bmatrix} -\psi_{f1}\sin\theta \\ \psi_{f1}\cos\theta \\ -3\psi_{f3}\sin 3\theta \\ 3\psi_{f3}\cos 3\theta \end{bmatrix} \tag{1}$$

where L_{m1} is the rated value of first harmonic inductance in the α-β subspace, L_{m3} is the rated value of third harmonic inductance in the x-y subspace, Ψ_{f1} is the rated value of first harmonic rotor flux linkage in the α-β subspace, Ψ_{f3} is the rated value of third harmonic rotor flux linkage in the x-y

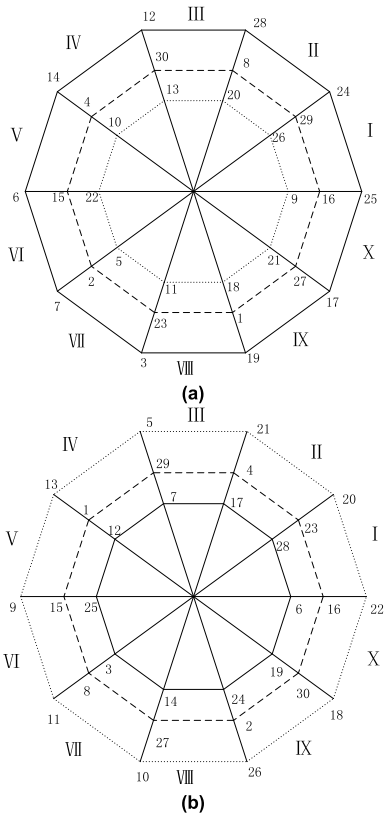

FIGURE 1. Voltage vectors of 5P-PMSM. (a) α-β subspace. (b) *x-y* subspace.

subspace; R is the rated value of phase resistance; θ is the rotor position of the motor.

A. SYNTHESIS OF VIRTUAL VOLTAGE VECTOR GROUP

A 5-phase voltage source inverter(VSI) is used to power the 5P-PMSM. The inverter can produce 32 primary voltage vectors that fall into four categories according to their amplitudes in the α-β subspace, i.e.:

I). Small-vectors($0.2472u_{dc}$) is acquired when the high-side (or low-side) switches of the two non-adjacent phases of the inverter are conducting simultaneously.

II). Medium-vectors($0.4u_{dc}$) is acquired when the high-side (or low-side) switches of the single phases of the inverter are conducting.

III). Large-vectors($0.6472u_{dc}$) is acquired when the high-side (or low-side) switches of two adjacent phases of the inverter are conducting jointly.

IV). Zero vectors are acquired when all the high-side (or low-side) switches of the inverter are conducting. (note: u_{dc} stands for the bus voltage magnitude.).

Any voltage space vector in the α-β subspace has its unique voltage vector in the *x-y* subspace, and its phase angle is three times the voltage vector in the α-β subspace.

In the *x-y* subspace, the amplitude of the concomitant voltage vector of the medium vectors remains unchanged. Magnitudes of the concomitant voltage vectors of the large and small vectors in the *x-y* subspace are 0.2472 u_{dc} and 0.6472 u_{dc}, respectively. According to the phases and amplitudes of the 32 voltage vectors in the two spaces, the voltage vector diagrams of the α-β subspace and the *x-y* subspace can be obtained, as shown in Fig 1. In FCS-MPCC, all the voltage vectors of the voltage vector group are brought into the 5P-PMSM prediction model in one control period and optimized the most suitable voltage vector according to the cost function. 5P-PMSM has 32 primary voltage vectors. Therefore, it is essential to select the voltage vector group reasonably. In this article, *a* large vector and a medium vector of the same phase angle in the α-β coordinate system are chosen to form a virtual vector to reduce the computational burden, and the action time ratio of the two primary voltage vectors is λ. It can be seen from Fig.1 that there are ten such virtual voltage vectors, which form a voltage vector group. According to Fig. 1, the large and medium vectors with the same phase angle in the α-β subspace have corresponding voltage vectors in the *x-y* subspace. The phase angles of these associated voltage vectors differ by 180°. When the value of λ is equal to 1.618, the amplitude of the virtual voltage vector in the α-β subspace is the largest, 0.5528 u_{dc}, and the amplitude of the associated voltage vector is zero in the *x-y* subspace. Hence, the third harmonic component in the prediction model and the cost function can be omitted. The virtual voltage vector group used in this paper is shown in Table 1.

TABLE 1. Virtual voltage vector group.

x	*Synthetic based vector*	u_α	u_β	u_x	u_y
1	16、25	$0.5528u_{dc}$	0	0	0
2	24、29	$0.4472u_{dc}$	$0.325u_{dc}$	0	0
3	8、28	$0.17u_{dc}$	$0.5258u_{dc}$	0	0
4	30、12	$-0.17u_{dc}$	$0.5258u_{dc}$	0	0
5	4、14	$-0.4472\ u_{dc}$	$0.325u_{dc}$	0	0
6	15、6	$-0.5528u_{dc}$	0	0	0
7	2、7	$-0.4472u_{dc}$	$-0.325u_{dc}$	0	0
8	23、3	$-0.17u_{dc}$	$-0.5258u_{dc}$	0	0
9	1、19	$0.17u_{dc}$	$-0.5258u_{dc}$	0	0
10	27、17	$0.4472u_{dc}$	$-0.325u_{dc}$	0	0

B. OPTIMUM VOLTAGE VECTOR OPTIMIZATION PROCESS

Euler method is used to discretize the fundamental harmonic mathematic model in (1):

$$\begin{bmatrix} i_\alpha(k+1) \\ i_\beta(k+1) \end{bmatrix} = (1 - R\frac{T_s}{L_{m1}}) \begin{bmatrix} i_\alpha(k) \\ i_\beta(k) \end{bmatrix} + \frac{T_s}{L_{m1}} \left(\begin{bmatrix} u_\alpha(k) \\ u_\beta(k) \end{bmatrix} - \psi_{f1}\omega_e(k) \begin{bmatrix} -\sin\theta(k) \\ \cos\theta(k) \end{bmatrix} \right) \quad (2)$$

To compensate for one beat delay, the output voltage vector, the rotor position, and the sampling values of current and speed can be substituted into (3) to calculate the current

prediction value of the next beat.

$$\begin{bmatrix}\hat{i}_\alpha(k+1)\\ \hat{i}_\beta(k+1)\end{bmatrix} = (1-\frac{RT_s}{L_{m1}})\begin{bmatrix} i_\alpha(k)\\ i_\beta(t)\end{bmatrix} + \frac{T_s}{L_{m1}}(\begin{bmatrix} u_{\alpha\_opt}(k)\\ u_{\beta\_opt}(k)\end{bmatrix} - \psi_{f1}\omega_e(k)\begin{bmatrix}-\sin\theta(k)\\ \cos\theta(k)\end{bmatrix}) \quad (3)$$

Bring (3) into (2) to get the compensated mathematic model of 5P-PMSM:

$$\begin{bmatrix}\hat{i}_\alpha[x](k+2)\\ \hat{i}_\beta[x](k+2)\end{bmatrix} = (1-\frac{RT_s}{L_{m1}})\begin{bmatrix}\hat{i}_\alpha(k+1)\\ \hat{i}_\beta(k+1)\end{bmatrix} + \frac{T_s}{L_{m1}}(\begin{bmatrix} u_\alpha[x]\\ u_\beta[x]\end{bmatrix} - \psi_{f1}\omega_e(k)\begin{bmatrix}-\sin\hat{\theta}(k+1)\\ \cos\hat{\theta}(k+1)\end{bmatrix}) \quad (4)$$

where $x = \{1, 2, \ldots, 10\}$, which is the serial number of the virtual voltage vector in Table 1, $\hat{\theta}(k+1)$ is position predicted value.

$$\hat{\theta}(k+1) = \theta(k) + \omega_e(k) * T_s$$

The cost function is shown in (5)

$$g_{basic} = \left|i^*_\alpha(k+2) - \hat{i}_\alpha[x](k+2)\right| + \left|i^*_\beta(k+2) - \hat{i}_\beta[x](k+2)\right| \quad (5)$$

Bring all the virtual voltage vectors in Table 1 into (4) in turn to obtain the current prediction value at $(k+2)$-th under different voltage vector excitation, and bring the prediction results into (5), respectively. The voltage vector corresponding to the smallest value of the g_{basic} is the optimal voltage vector.

C. CALCULATION OF ACTION TIME OF THE VIRTUAL VOLTAGE VECTOR

As the 5P-PMSM works under different load (or speed) conditions, the expected voltage vector amplitude also changes accordingly. When the motor operates under light load or at low speed, the expected voltage vector amplitude is smaller than the virtual voltage vector amplitude. In one period, the actual current variation is higher than the reference current variation, which leads the actual current jitter around the reference current. The smaller the expected amplitude of the voltage vector is, the more pronounced the chattering phenomenon is. Take i_α as an example, as shown in Fig.2. The solid blue line is the reference current. The solid red line is the actual current under the action of the optimal voltage vector when the expected amplitude of the voltage vector is smaller than the amplitude of the optimal voltage vector. Moreover, the red dashed line is the predicted current under the action of the non-optimal vector. $i_{\Delta\alpha}$ stands for the error between the actual current value and the reference current.

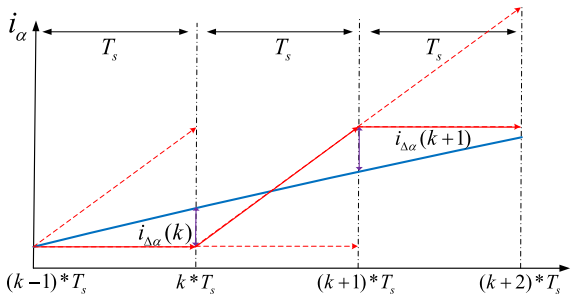

FIGURE 2. i_α real current and reference current.

By optimizing the action time of the optimal voltage vector, the equivalent amplitude regulation of the optimal voltage vector in a single period is realized, thus reducing the chattering phenomenon in the current waveform. According to the current reference value at $(k+2)$-th and the predicted value of rotor position and current at $(k+1)$-th, the corresponding expected voltage vector at $(k+2)$-th could be obtained:

$$\begin{bmatrix}u^*_\alpha(k+2)\\ u^*_\beta(k+2)\end{bmatrix} = \frac{L_{m1}}{T_s}\begin{bmatrix}i^*_\alpha(k+2)\\ i^*_\beta(k+2)\end{bmatrix} - (\frac{L_{m1}}{T_s} - R)\begin{bmatrix}\hat{i}_\alpha(k+1)\\ \hat{i}_\beta(k+1)\end{bmatrix} + \psi_{f1}\omega_e(k)\begin{bmatrix}-\sin\hat{\theta}(k+1)\\ \cos\hat{\theta}(k+1)\end{bmatrix} \quad (6)$$

Bring the expected voltage vector into (7); the desired voltage vector amplitude is obtained. According to Table 1, the amplitude of the voltage vector is $0.5528u_{dc}$. The amplitude of the inverter output voltage vector is adjusted by modifying the action time within a single period. When the amplitude of the inverter output voltage vector is equal to the desired voltage vector amplitude in (7), the action time is optimal, and the current chattering phenomenon is minimized.

$$u^*_{\alpha\beta}(k+2) = \sqrt{(u^*_\alpha(k+2))^2 + (u^*_\beta(k+2))^2} \quad (7)$$

Bring the desired voltage vector amplitude into (8), the corresponding optimal action time t_{ed} at $(k+2)$-th can be obtained:

$$t_{ed} = \frac{u^*_{\alpha\beta}(k+2)}{0.5528u_{dc}}T_s \quad (8)$$

Using t_{ed} to replace the virtual voltage vector action time T_s in (4). By controlling t_{ed}, the prediction model for the adjustment of voltage vector amplitude is realized:

$$\begin{bmatrix}\hat{i}_\alpha[x](k+2)\\ \hat{i}_\beta[x](k+2)\end{bmatrix} = (1-\frac{RT_s}{L_{m1}})\begin{bmatrix}\hat{i}_\alpha(k+1)\\ \hat{i}_\beta(k+1)\end{bmatrix} + \frac{t_{ed}}{L_{m1}}\begin{bmatrix}u_\alpha[x]\\ u_\beta[x]\end{bmatrix} - \frac{T_s}{L_{m1}}\psi_{f1}\omega_e(k)\begin{bmatrix}-\sin\hat{\theta}(k+1)\\ \cos\hat{\theta}(k+1)\end{bmatrix} \quad (9)$$

III. EFFECT OF MOTOR PARAMETERS ON FCS-MPCC FOR 5F-PMSM

There are errors between the measured and rated value of motor parameters:

$$\begin{cases} R_c = R + \Delta R \\ L_{cm1} = L_{m1} + \Delta L \\ \psi_{cf1} = \psi_{m1} + \Delta\psi \end{cases} \tag{10}$$

where R_c is the measured resistance value; ΔR is the resistance error value; L_{cm1} is the measured value of first harmonic inductance in the α-β subspace; ΔL is the error value of first harmonic inductance in the α-β subspace; Ψ_{cf1} is the measured value of first harmonic flux linkage in the α-β subspace; $\Delta\Psi$ is the error value of first harmonic flux linkage in the α-β subspace.

A. SYNTHESIS OF VIRTUAL VOLTAGE VECTOR GROUP

According to (6), when the estimated value of current at the $(k+2)$-*th* in (9) is the closest to the reference value, the corresponding virtual voltage vector is the optimal voltage vector. It is assumed that the current prediction value at the $(k+2)$-*th* is equal to the reference value, replacing the rated value of the parameter in (9) with the measured value in (10), the expression of optimal voltage vector at the $(k+2)$-*th* is obtained:

$$\begin{aligned} &\frac{t_{ed}}{T_s}\begin{bmatrix} u_{\alpha-opt}(k+2) \\ u_{\beta-opt}(k+2) \end{bmatrix} \\ &= \underbrace{\frac{L_{cm1}}{T_s}\begin{bmatrix} i^*_\alpha(k+2) - i^*_\alpha(k+1) \\ i^*_\beta(k+2) - i^*_\beta(k+1) \end{bmatrix}}_{term_1} \\ &\quad + \underbrace{R_c\begin{bmatrix} i^*_\alpha(k+1) \\ i^*_\beta(k+1) \end{bmatrix}}_{term_2} + \underbrace{\psi_{cf1}\omega_e(t)\begin{bmatrix} -\sin\theta(k+1) \\ \cos\theta(k+1) \end{bmatrix}}_{term_3} \end{aligned} \tag{11}$$

Equation (11) is consists of three parts. Among them, $term_1$ is affected by the measured value of first harmonic inductance and the variation of current in one period; $term_2$ is affected by the resistance measurement value and the current value at the $(k+1)$-*th*; $term_3$ is affected by the measured value of first harmonic flux linkage. According to (11), the reference current and back electromotive force is determined by the rotor position. Therefore, when Ψ_{cf1} is higher than Ψ_{f1} (or R_c is higher than R), the proportion of $team_2$ and $team_3$ in (11) increase, and optimization results of the optimal voltage vector are more sensitive to the rotor position. However, when L_{cm1} is higher than L_{m1}, the proportion of $team_1$ in (11) increased. Optimization results of the optimal voltage vector are more sensitive to the variation of current in one period, which leads to an increase in the actual current chattering or even causing a mismatch between rotor position and current phase.

B. INFLUENCE OF PARAMETER MISMATCH ON t_{ed} calculation

When the parameter measured value is higher than the rated value, the calculated result is higher than the expected value, according to (11). So the action time of the optimal voltage vector is higher than the optimal action time, which results in the current rate of change in one period is higher than the expected values.

Because of the adverse effects of parameter mismatch on the control performance of FCS-MPCC in these two aspects, a stator current and concentration disturbance observer (SCCDO) can simultaneously predict the next beat current value and track concentrated disturbance in the prediction model, is proposed.

IV. CURRENT LOOP CONTROL BASED ON FCS-MPCC+SCCDO

A. SCCDO BASED ON VG-STA ALGORITHM

Substitute (10) into the first harmonic math model in (1).

$$\begin{bmatrix} \frac{di_\alpha}{dt} \\ \frac{di_\beta}{dt} \end{bmatrix} = \frac{1}{L_{cm1}}\left(\begin{bmatrix} u_\alpha \\ u_\beta \end{bmatrix} - R_c\begin{bmatrix} i_\alpha \\ i_\beta \end{bmatrix} - \omega_e\psi_{cf1}\begin{bmatrix} -\sin\theta \\ \cos\theta \end{bmatrix} + \begin{bmatrix} \Gamma_\alpha \\ \Gamma_\beta \end{bmatrix}\right) \tag{12}$$

where: Γ_α and Γ_β represent parameter concentrated disturbance of the α-axis and β-axis, respectively:

$$\begin{bmatrix} \Gamma_\alpha \\ \Gamma_\beta \end{bmatrix} = \Delta R\begin{bmatrix} i_\alpha \\ i_\beta \end{bmatrix} + \omega_e\Delta\psi\begin{bmatrix} -\sin\theta \\ \cos\theta \end{bmatrix} + \Delta L\begin{bmatrix} \frac{di_\alpha}{dt} \\ \frac{di_\beta}{dt} \end{bmatrix}$$

The SCCDO can be designed as follows:

$$\begin{bmatrix} \frac{d\hat{i}_\alpha}{dt} \\ \frac{d\hat{i}_\beta}{dt} \end{bmatrix} = \frac{1}{L_{m1}}\left(\begin{bmatrix} u_\alpha \\ u_\beta \end{bmatrix} - R\begin{bmatrix} \hat{i}_\alpha \\ \hat{i}_\beta \end{bmatrix} - \omega_e\psi_{m1}\begin{bmatrix} -\sin\theta \\ \cos\theta \end{bmatrix} - \begin{bmatrix} \hat{\Gamma}_\alpha \\ \hat{\Gamma}_\beta \end{bmatrix}\right) \tag{13}$$

where: $\hat{\Gamma}_\alpha$ and $\hat{\Gamma}_\beta$ represent the estimated value of parameter concentrated disturbance of the α-axis and β-axis, respectively:

$$\begin{bmatrix} \hat{\Gamma}_\alpha \\ \hat{\Gamma}_\beta \end{bmatrix} = \Delta R\begin{bmatrix} i_\alpha \\ i_\beta \end{bmatrix} + \omega_e\Delta\psi\begin{bmatrix} -\sin\theta \\ \cos\theta \end{bmatrix} + \Delta L\begin{bmatrix} \frac{di_\alpha}{dt} \\ \frac{di_\beta}{dt} \end{bmatrix}$$

According to (12) and (13), the error equation between the prediction model and the actual model can be obtained as:

$$\frac{de_\tau}{dt} = -\frac{R_c}{L_{cm1}}e_\tau - \frac{1}{L_{cm1}}(\hat{\Gamma}_\tau - \Gamma_\tau) \tag{14}$$

where: $e_\tau = \hat{i}_\tau - i_\tau$, $\tau \in \{\alpha, \beta\}$.

The sliding-mode surface is chosen:

$$s_\tau = \hat{i}_\tau - i_\tau \tag{15}$$

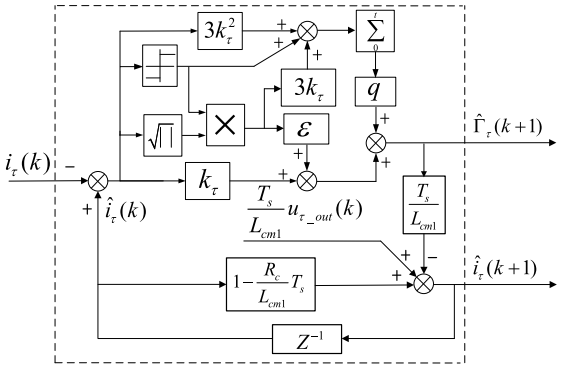

FIGURE 3. Discrete block diagram of proposed SCCDO.

When the state variables converge to the sliding mode surface, the concentrated disturbance's estimated value can genuinely reflect the parameter mismatch that exists in the prediction model. The VG-STA algorithm was selected as the concentrated disturbance estimation function, as shown in (16).The proposed algorithm consists of two parts: proportional ($term_4$ in equation (16))and integral($term_5$ in equation (16)). The value of s_τ is both positive and negative.

In order to obtain the square root of s_τ, the sign function is introduced into the algorithm. The role of the sign function in VG-STA is different from that in first-order sliding mode.

Therefore, the chattering of sliding mode variables along the sliding mode surface will not occur. Compare with the traditional STA, VG-STA increases the proportion of sliding mode variable, which can improve the convergence speed by adjusting the proportional coefficient k_τ. k_τ is a constant greater than zero.

$$\hat{\Gamma}_\tau = \varepsilon \underbrace{(\sqrt{|s_\tau|}sign(s_\tau) + k_\tau s_\tau)}_{term_4} + q\underbrace{\int (\sqrt{|s_\tau|}sign(s_\tau)+k_\tau s_\tau)\cdot(1/2\sqrt{|s_\tau|}+k_\tau)dt}_{term_5} \quad (16)$$

1) OBSERVER STABILITY ANALYSIS

Assuming the concentrated disturbance meets the Lipschitz continuous condition and the derivative of concentrated disturbance along the time axis exists. Take (16) into (14).

$$\dot{s}_\tau = -\frac{\varepsilon}{L_{cm1}}(\sqrt{|s_\tau|}sign(s_\tau) + k_\tau s_\tau) - \frac{R_c}{L_{cm1}}s_\tau + \phi(s_\tau) \quad (17)$$

where: $\phi(s_\tau) = \int \dot{\Gamma}_\tau - q(\sqrt{|s_\tau|}sign(s_\tau) + k_\tau s_\tau)\cdot(1/2\sqrt{|s_\tau|}+k_\tau)dt$.

To prove the stability of (17), establish a quadratic Lyapunov function $v(s_\tau, \phi(s_\tau))$:

$$v(s_\tau, \phi(s_\tau)) = \zeta^T P\zeta \quad (18)$$

where: $\zeta = \begin{bmatrix} \sqrt{|s_\tau|}sign(s_\tau) + k_\tau s_\tau \\ \phi(s_\tau) \end{bmatrix}$, $P = \begin{bmatrix} \kappa_1 + 4\kappa_2^2 & -2\kappa_2 \\ -2\kappa_2 & 1 \end{bmatrix}$ with arbitrary positive constants $\kappa 1 > 0, \kappa 2 > 0$.

The derivative of ζ along the time is shown as:

$$\dot{\zeta} = \eta A\zeta \quad (19)$$

where: $A = \begin{bmatrix} -\frac{\varepsilon}{L_{cm1}} & -\frac{R_c s_\tau}{L_{cm1}\zeta_1}1 \\ -\frac{q}{L_{m1}} & +\frac{\Gamma_\tau}{L_{m1}\zeta_1\eta}0 \end{bmatrix}$, $\eta = (\frac{1}{2\sqrt{|s_\tau|}} + k_\tau)$

The derivative of $v(s_\tau, \phi(s_\tau))$ along the time:

$$\dot{v}(s_\tau, \phi(s_\tau)) = \eta\zeta^T(A^T P + PA)\zeta \le -\eta\zeta^T Q\zeta$$

$$Q = \begin{bmatrix} 2(\frac{\varepsilon}{L_{cm1}} + \frac{R_c s_\tau}{L_{cm1}\zeta_1})(\kappa_1 + 4\kappa_2^2) - 4\kappa_2(\frac{q}{L_{m1}} - \frac{\dot{\Gamma}_\tau}{L_{m1}\zeta_1\eta}) & \blacktriangle \\ -(\kappa_1 + 4\kappa_2^2) - 2\kappa_2(\frac{\varepsilon}{L_{cm1}} + \frac{R_c s_\tau}{L_{cm1}\zeta_1}) + (\frac{q}{L_{m1}} - \frac{\Gamma_\tau}{L_{m1}\zeta_1\eta})4\kappa_2 \end{bmatrix} \quad (20)$$

where: $|\dot{\Gamma}_\tau / L_{m1}\zeta_1\eta| \le \delta_1$, $|R_c s_\tau / L_{cm1}\zeta_1| \le \delta_2$, $\blacktriangle$ is used to indicate a symmetric element.

To make the observer corresponding to (17) satisfies the Lyapunov global asymptotic stability condition, the Q in (20) must be a positive definite symmetric matrix. Hence, the selection of the parameters ε and q in (16) is shown in formula (21).

$$\begin{cases} q = L_{m1}(\kappa_1 + 4\kappa_2^2) + 2\kappa_2\varepsilon \\ \varepsilon = \dfrac{L_{cm1}}{\kappa_1}\begin{pmatrix} \dfrac{1}{4\kappa_2}(2\kappa_2\delta_2 + \delta_1)^2 + \kappa_2 \\ -2\kappa_2\delta_1 - (\delta_2 - 2\kappa_2)(\kappa_1 + 4\kappa_2^2) \end{pmatrix} \end{cases} \quad (21)$$

Take (21) into Q in formula (20):

$$\dot{v}(s_\tau, \phi(s_\tau)) = -\eta\zeta^T Q\zeta \le -2\kappa_2\eta\zeta^T\zeta \quad (22)$$

2) DISCRETIZATION PROCESS

Taking the optimal current-voltage vector and the back electromotive force as a whole, which acts on the motor winding, as shown in (23).

$$\begin{bmatrix} u_{\alpha\_out}(k) \\ u_{\beta\_out}(k) \end{bmatrix} = \frac{t_{ed}}{T_s}\begin{bmatrix} u_{\alpha\_opt}(k) \\ u_{\beta\_opt}(k) \end{bmatrix} - \psi_{cf1}\omega_e(k)\begin{bmatrix} -\sin\theta(k) \\ \cos\theta(k) \end{bmatrix} \quad (23)$$

Euler method is used to discretize (13) and (16), and then the discrete form of SCCDO based on the VG-STA algorithm is obtained:

$$\hat{i}_\tau(k+1) = \frac{T_s}{L_{cm1}}u_{\tau\_out}(k) + (1 - \frac{R_c T_s}{L_{cm1}})i_\tau(k) + \frac{T_s}{L_{cm1}}\hat{\Gamma}_\tau(k+1) \quad (24)$$

where:

$$\hat{\Gamma}_\tau(k+1) = \varepsilon(\sqrt{|s_\tau(k)|}sign(s_\tau(k)) + k_r s_\tau(k)) + qT_s\sum_0^t(\sqrt{|s_\tau|}sign(s_\tau(k)) + k_\tau s_\tau(k))\cdot(1/2\sqrt{|s_\tau(k)|} + k_\tau)$$

According to (23) and (24), the discrete block diagram of SCCDO is illustrated in Fig. 3.

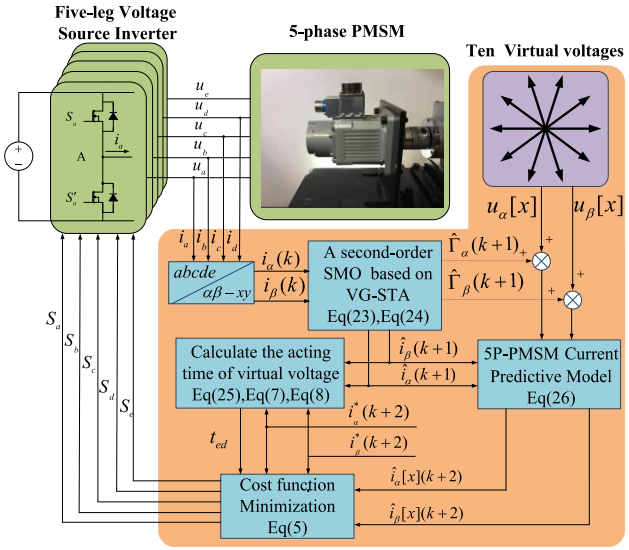

FIGURE 4. Block diagram of a 5P-PMSM drive system based on FCS-MPCC+SCCDO.

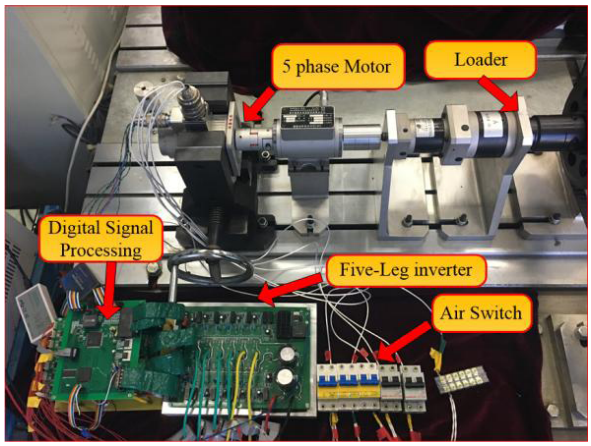

FIGURE 5. Experimental test platform.

B. FCS-MPCC WITH SCCDO

Firstly, five-phase current sample values are subjected to Clark transformation to obtain i_α, i_β. The SCCDO takes i_α and i_β as its inputs to generate the predicted value of current and the observed value of concentration disturbance for the next moment.

$$\begin{bmatrix} u_\alpha^*(t+2) \\ u_\beta^*(t+2) \end{bmatrix} = R_c \begin{bmatrix} \hat{i}_\alpha(t+1) \\ \hat{i}_\beta(t+1) \end{bmatrix} + \psi_{f1}\omega_e(t) \begin{bmatrix} -\sin\theta(t+1) \\ \cos\theta(t+1) \end{bmatrix} + \frac{L_{cm1}}{T_s} \begin{bmatrix} i_\alpha^*(t+2) - \hat{i}_\alpha(t+1) \\ i_\beta^*(t+2) - \hat{i}_\beta(t+1) \end{bmatrix} + \begin{bmatrix} \hat{\Gamma}_\alpha(t+1) \\ \hat{\Gamma}_\beta(t+1) \end{bmatrix} \quad (25)$$

Secondly, the observed results are substituted into (25) to obtain the compensated expected voltage vector at $(k+1)$-*th*.Then, the compensated expected voltage vector is brought into (7) and (8) to get the value of t_{ed}. Finally, the current predicted value, the observation value of concentration disturbance, t_{ed}, and ten virtual voltage vectors

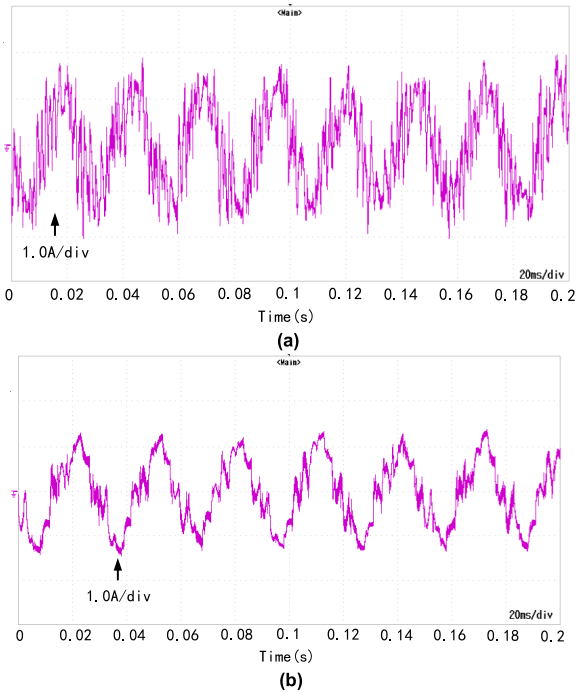

FIGURE 6. A-phase current waveform at different action times. (a) T_s (b) t_{ed}.

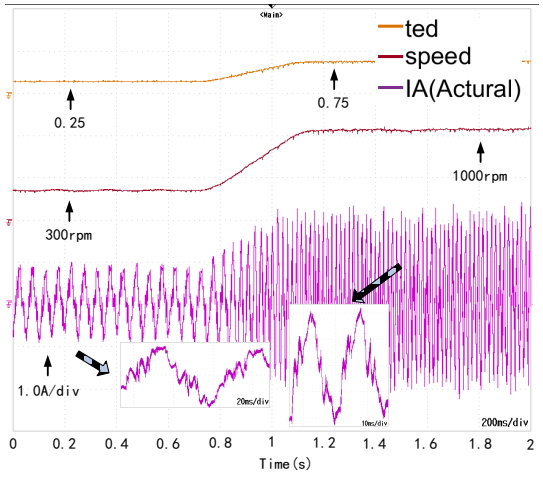

FIGURE 7. The value of ted with the increase of speed and load torque.

in Table 1 are sequentially brought into (26), and ten current estimate value is obtained at $(k+2)$-*th* correspondingly. Bring ten current estimate value into (5) in turn, and the optimal voltage vector is obtained. The entire control process of FCS-MPCC+SCCDO is shown in Fig.4.

$$\begin{bmatrix} \hat{i}_\alpha[x](k+2) \\ \hat{i}_\beta[x](k+2) \end{bmatrix} = (1 - \frac{RT_s}{L_{m1}}) \begin{bmatrix} \hat{i}_\alpha(k+1) \\ \hat{i}_\beta(k+1) \end{bmatrix} + \frac{T_s}{L_{m1}} \begin{bmatrix} \hat{\Gamma}_\alpha(k+1) \\ \hat{\Gamma}_\beta(k+1) \end{bmatrix} + \frac{T_s}{L_{m1}} (\frac{t_{ed}}{T_s} \begin{bmatrix} u_\alpha[x] \\ u_\beta[x] \end{bmatrix} - \psi_{f1}\omega_e(t) \begin{bmatrix} -\sin\hat{\theta}(k+1) \\ \cos\hat{\theta}(k+1) \end{bmatrix}) \quad (26)$$

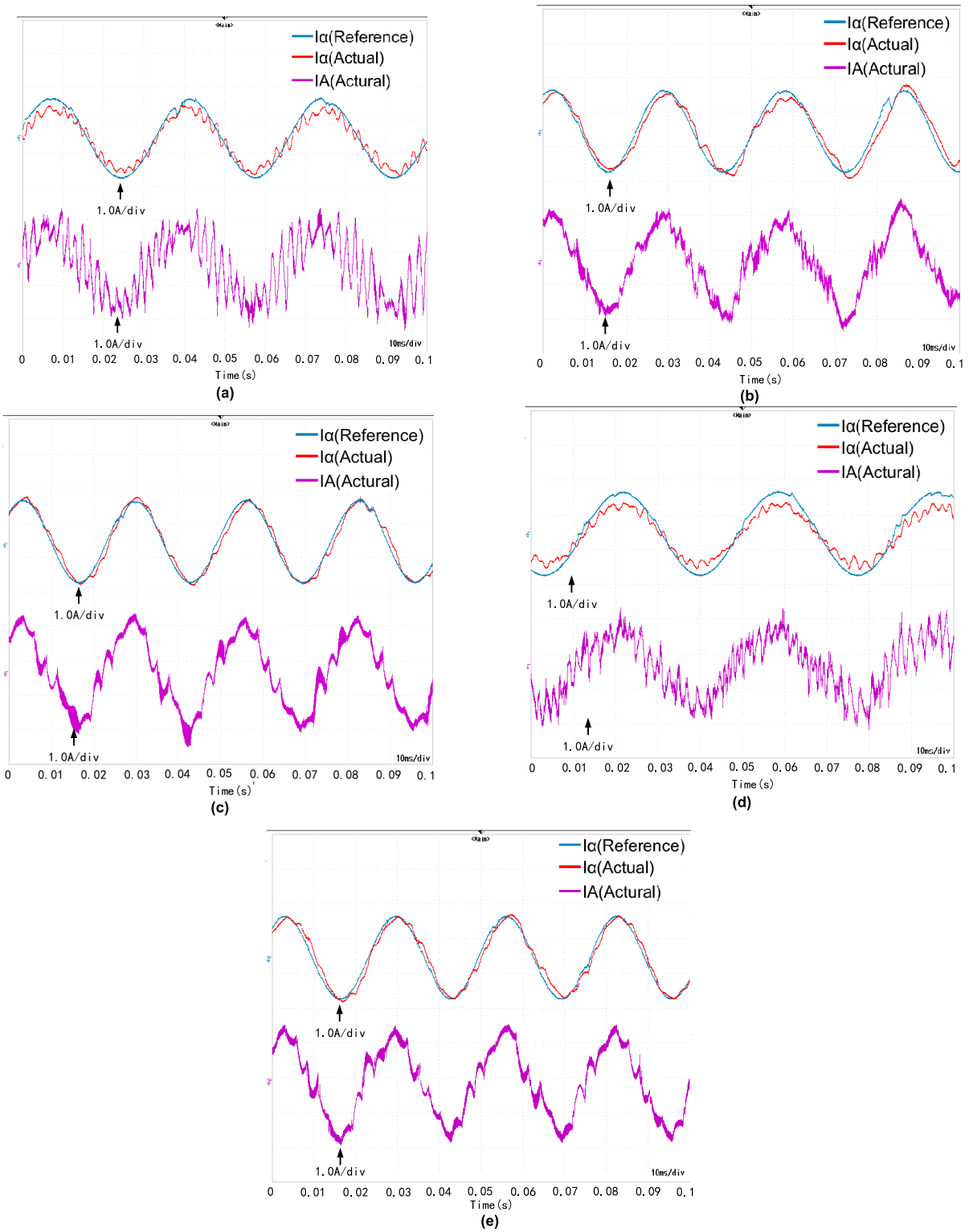

FIGURE 8. Current Waveform of FCS-MPC under parameter mismatch. (a)$L_{cm1}=2L_{m1}$.(b)$L_{cm1}=0.5L_{m1}$.(c)$\Psi c_{f1}=2\Psi_{f1}$.(d)$\Psi c_{f1}=0.5\Psi_{f1}$.(e)R_c = 10R.

V. PRESENTATION OF RESULTS

In this section, to demonstrate the effectiveness of the proposed predictive current control approach, experiments of the MPCC method and the MPCC +SCCDO method of the 5P-PMSM system were carried out. The central control unit based on TMS320F28335 of TI Company is used to realize

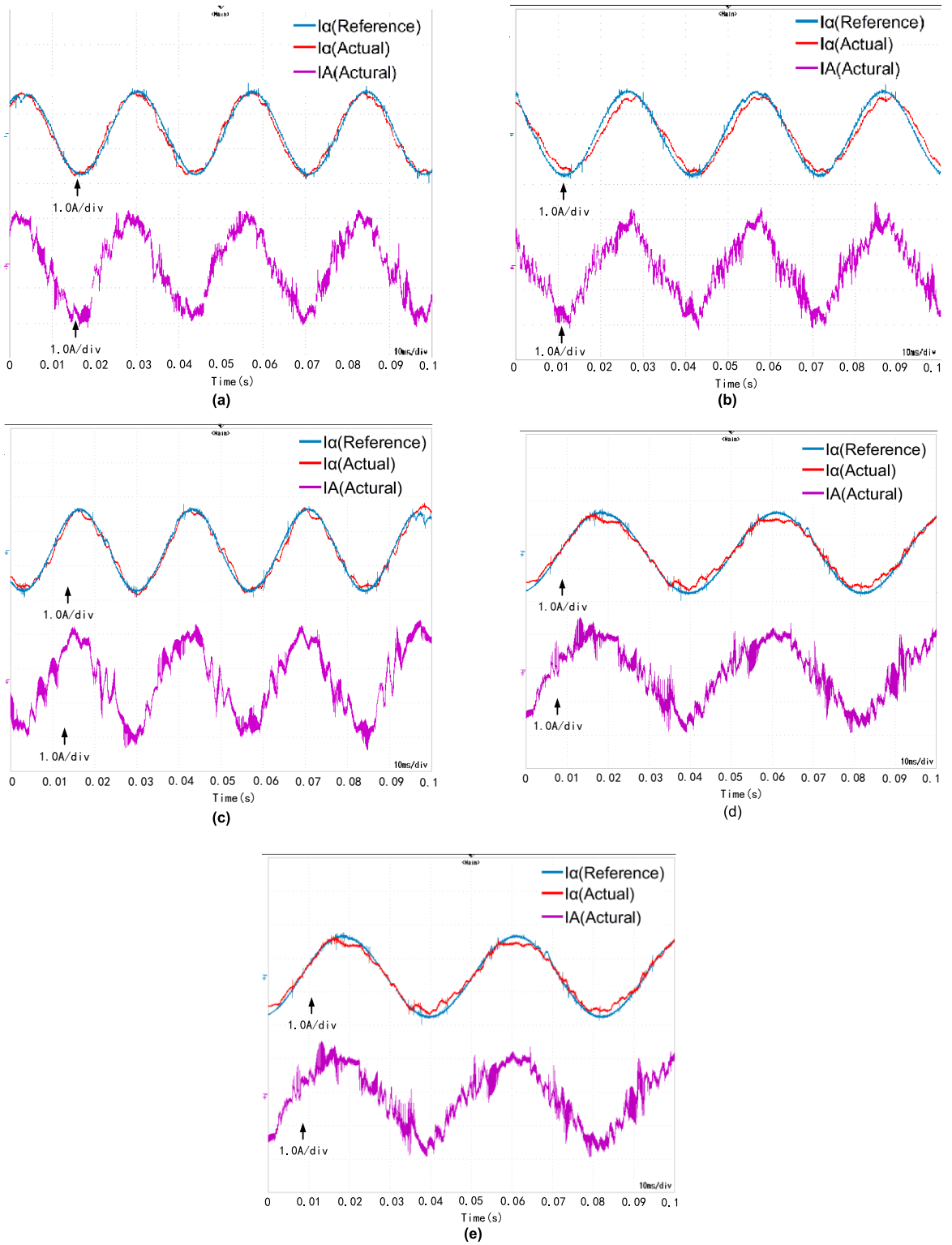

FIGURE 9. Current Waveform of FCS-MPC +SCCDO under parameter mismatch.(a)$L_{cm1} = 2L_{m1}$.(b)$L_{cm1} = 0.5L_{m1}$.(c)$\Psi c_{f1} = 2\Psi_{f1}$.(d) $\Psi c_{f1} = 0.5\Psi_{f1}$.(e) R_c = 10R.

FCS-MPCC+SCCDO. Moreover, the current loop control frequency is 10 kHz. The experimental test platform is shown in Fig.5, and the experimental motor parameters are shown in Table 2.

In order to evaluate the algorithm for the optimal action time, a comparative experiment was carried out. The experimental results are shown in Fig.6, where the virtual voltage's action time is set as T_s and t_{ed}, respectively. The reference

TABLE 2. FP-PMSM parameters.

Parameter	Value	Parameter	Value
DC-link voltage	96V	Winding pattern	Single-Layer Fractional-Slot Concentrated Winding
Pair of poles	4	R	0.52Ω
L_{m1}	1.2mH	L_{m3}	0.02mH
ψ_{f1}	0.0163V·s	ψ_{f3}	0.000094V·s

speed is 500 rpm, and the load torque is 0.5N.m. In this case, the optimal action time of the virtual voltage vector t_{ed} is 0.4424 T_s.

Adjusting the virtual voltage action time is equivalent to adding a zero voltage vector in one control period. The addition of the zero voltage vector in one period can reduce current fluctuations, which could be confirmed by comparing (a) and (b) in Fig.6. The fluctuations in A-phase current waveform are minimized when the action time equals t_{ed}.

To verify the dynamic performance of the t_{ed} calculation method proposed in this paper, the 5P-PMSM operates in the ramp-up stage. The load torque also increases as the speed increases. The experimental waveform is shown in Fig. 7 that corresponds to speed (brown line), t_{ed} (green line), and phase A current (purple line). Initially, the 5P-PMSM speed was set at 300 rpm, the load torque was 0.3 N.m, and the corresponding t_{ed} was 0.25.

To ensure the chattering in the A-phase current waveform is the minimum, the value of t_{ed} increases with increasing the speed and load torque. When the speed reaches 1000 rpm, the load torque is 0.7N.m, and the corresponding t_{ed} is 0.75.

The current reference values of the 5P-PMSM current loop is set as $i_q* = 1.5A, i_d* = 0$, and load torque is 0.5N.m. The current loop adopted two control methods (FCS-MPCC, FCS-MPCC+SCCDO) under the prediction model's parameter mismatch. The experimental results are Fig.8 and Fig.9, respectively, corresponding to the α-axis reference current (blue line), α-axis current (red line), and phase A current (purple line). By comparing the current waveforms of α-axis (and phase A) under different parameters mismatch conditions in Fig.8, the following conclusions can be given:

1)When the measured value and rated value of the three parameters of inductance, flux linkage, and resistance satisfy anyone or several conditions in (27), the fluctuation of the α-axis current (and the phase A) current significantly increases.

$$\begin{cases} L_{cm1} > L_{m1} \ or \ \psi_{cf1} < \psi_{f1} \\ or \ R_c < R \end{cases} \tag{27}$$

2)When the measured value and rated value of the three parameters of inductance, flux linkage, and resistance satisfy anyone or several conditions in (28), it leads to the optimization result of the optimal voltage vector being more inclined to the rotor position, and current tracking ability is weakened.

$$\begin{cases} L_{cm1} < L_{m1} \ or \ \psi_{cf1} > \psi_{f1} \\ or \ R_c > R \end{cases} \tag{28}$$

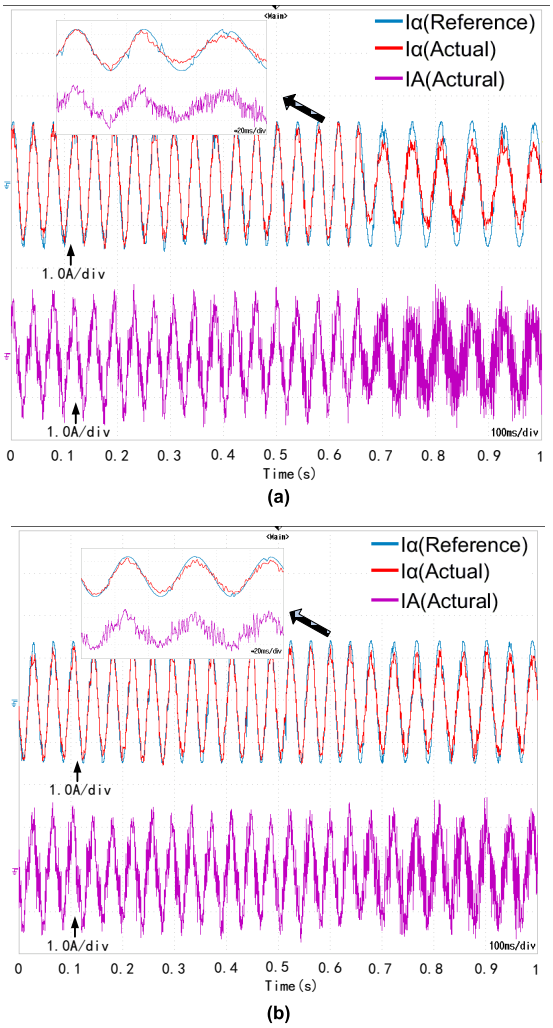

FIGURE 10. Current Waveform when a step change of parameter occurs (from Ψ_{f1} and L_{m1} change to $0.5\Psi_{f1}$ and $2L_{m1}$). (a) FCS-MPCC. (b) FCS-MPCC +SCCDO.

From the experimental results, it can be seen that the influence of the motor parameter mismatch on the control performance of FCS-MPC cannot be ignored. The parameter mismatch of flux linkage and inductance have opposite effects on control performance. Whereas the parameter mismatch of flux linkage and resistance have the same effect on control performance. The experimental results are consistent with the theoretical analysis.Fig.9 shows experimental results after the concentrated disturbance compensation under different parameter mismatch conditions. The parameters of the VG-STA algorithm in the experiment are $\varepsilon = 0.5, q = 2, k_\Gamma = 1$. Compared with the current waveform in Fig.8 at the same parameter mismatch conditions, it can be found that the current waveform has been significantly improved.

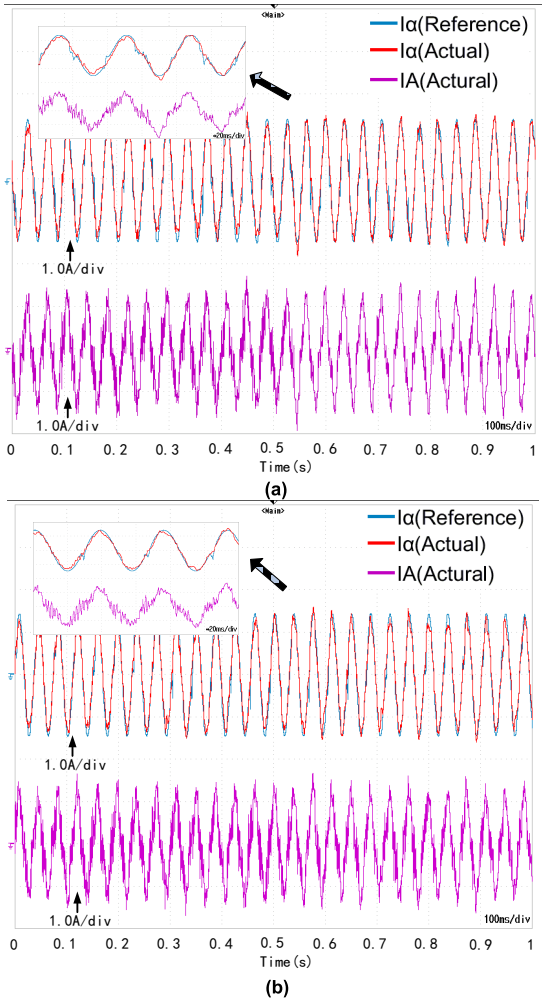

FIGURE 11. Current Waveform when a step change of parameter occurs (from Ψ_{f1} and L_{m1} change to $2\Psi_{f1}$ and $0.5L_{m1}$).(a) FCS-MPCC. (b) FCS-MPCC +SCCDO.

To further evaluate the dynamic performance of the proposed SCCDO, the experiment was completed when a step change of parameter during the operation.

Fig 10 and Fig 11 show the experiments' results when the motor parameters suddenly changed, and the current control uses FCS-MPCC and FCS-MPCC+SCCDO, respectively. From the results, it can be seen that the proposed SCCDO can quickly converge and compensate for the concentration disturbances caused by the step change of parameters during the system operation. According to experimental results, the SCCDO based on the AG-STA algorithm used in this paper can compensate concentrated disturbances in real-time, and improve the optimization results of the optimal voltage vector, and enhance current tracking performance in the case of parameter mismatches.

VI. CONCLUSION

In this paper, a novel FCS-MPCC method for 5P-PMSM is proposed to improve the current tracking ability and resiliency to parameter perturbations. The main contribution of this paper is as follows:

1).In order to suppress chattings in current waveform, a method used to calculate the optimal action time of voltage vector according to the motor model and work condition is presented;

2). From the perspective of optimal voltage vector selection, the influence of the motor parameter mismatch on the FCS-MPCC control effect is analyzed. On that basis, a second-order SMO algorithm based on AG-STA, which can predict the next beat current value and track concentrated disturbance in real-time, is proposed.

REFERENCES

[1] Z. Liu, Y. Li, and Z. Zheng, "A review of drive techniques for multiphase machines," *CES Trans. Electr. Mach. Syst.*, vol. 2, no. 2, pp. 243–251, Jun. 2018, doi: 10.30941/CESTEMS.2018.00030.

[2] C. Liu and Y. Luo, "Overview of advanced control strategies for electric machines," *Chin. J. Electr. Eng.*, vol. 3, no. 2, pp. 53–61, Sep. 2017, doi: 10.23919/CJEE.2017.8048412.

[3] Y. Zhang, B. Xia, H. Yang, and J. Rodriguez, "Overview of model predictive control for induction motor drives," *Chin. J. Electr. Eng.*, vol. 2, no. 1, pp. 62–76, Jun. 2016, doi: 10.23919/CJEE.2016.7933116.

[4] J. J. Aciego, I. G. Prieto, and M. J. Duran, "Model predictive control of six-phase induction motor drives using two virtual voltage vectors," *IEEE J. Emerg. Sel. Topics Power Electron.*, vol. 7, no. 1, pp. 321–330, Mar. 2019, doi: 10.1109/JESTPE.2018.2883359.

[5] I. Gonzalez-Prieto, M. J. Duran, J. J. Aciego, C. Martin, and F. Barrero, "Model predictive control of six-phase induction motor drives using virtual voltage vectors," *IEEE Trans. Ind. Electron.*, vol. 65, no. 1, pp. 27–37, Jan. 2018, doi: 10.1109/TIE.2017.2714126.

[6] Y. Luo and C. Liu, "Elimination of harmonic currents using a reference voltage vector based-model predictive control for a six-phase PMSM motor," *IEEE Trans. Power Electron.*, vol. 34, no. 7, pp. 6960–6972, Jul. 2019, doi: 10.1109/TPEL.2018.2874893.

[7] C. Xiong, H. Xu, T. Guan, and P. Zhou, "A constant switching frequency multiple-vector-based model predictive current control of five-phase PMSM with nonsinusoidal back EMF," *IEEE Trans. Ind. Electron.*, vol. 67, no. 3, pp. 1695–1707, Mar. 2020, doi: 10.1109/TIE.2019.2907502.

[8] Y. Zhang, Z. Yin, X. Sun, and Y. Zhong, "On-line identification methods of parameters for permanent magnet synchronous motors based on cascade MRAS," in *Proc. 9th Int. Conf. Power Electron. ECCE Asia (ICPE-ECCE Asia)*, Seoul, South Korea, Jun. 2015, pp. 345–350, doi: 10.1109/ICPE.2015.7167808.

[9] Z. Chen, J. Qiu, and M. Jin, "Adaptive finite-control-set model predictive current control for IPMSM drives with inductance variation," *IET Electr. Power Appl.*, vol. 11, no. 5, pp. 874–884, May 2017, doi: 10.1049/iet-epa.2016.0861.

[10] Z.-H. Liu, H.-L. Wei, X.-H. Li, K. Liu, and Q.-C. Zhong, "Global identification of electrical and mechanical parameters in PMSM drive based on dynamic self-learning PSO," *IEEE Trans. Power Electron.*, vol. 33, no. 12, pp. 10858–10871, Dec. 2018, doi: 10.1109/TPEL.2018.2801331.

[11] K. Liu and Z. Q. Zhu, "Quantum genetic algorithm-based parameter estimation of PMSM under variable speed control accounting for system identifiability and VSI nonlinearity," *IEEE Trans. Ind. Electron.*, vol. 62, no. 4, pp. 2363–2371, Apr. 2015, doi: 10.1109/TIE.2014.2351774.

[12] Z. Yin, X. Han, C. Du, J. Liu, and Y. Zhong, "Research on model predictive current control for induction machine based on immune-optimized disturbance observer," *IEEE J. Emerg. Sel. Topics Power Electron.*, vol. 6, no. 4, pp. 1699–1710, Dec. 2018, doi: 10.1109/JESTPE.2018.2820050.

[13] B. Jin, Y. Shen, and D. Wu, "Permanent magnet synchronous motor parameter identification with multi-innovation least squares," in *Proc. IEEE 11th Conf. Ind. Electron. Appl. (ICIEA)*, Hefei, China, Jun. 2016, pp. 752–757, doi: 10.1109/ICIEA.2016.7603682.

[14] R. Yang, M. Wang, L. Li, G. Wang, and C. Zhong, "Robust predictive current control of PMLSM with extended state modeling based Kalman filter: For time-varying disturbance rejection," *IEEE Trans. Power Electron.*, vol. 35, no. 2, pp. 2208–2221, Feb. 2020, doi: 10.1109/TPEL.2019.2923631.

[15] R. Shah and R. Gajjar, "A comparative study of various methods for parameter estimation of PMSM," in *Proc. Int. Conf. Energy, Commun., Data Anal. Soft Comput. (ICECDS)*, Chennai, India, 2017, pp. 1712–1715, doi: 10.1109/ICECDS.2017.8389742.

[16] M. De Soricellis, D. Da Ru, and S. Bolognani, "A robust current control based on proportional-integral observers for permanent magnet synchronous machines," *IEEE Trans. Ind. Appl.*, vol. 54, no. 2, pp. 1437–1447, Mar. 2018, doi: 10.1109/TIA.2017.2772171.
[17] Y. Zhang, Y. Bai, and H. Yang, "A universal multiple-vector-based model predictive control of induction motor drives," *IEEE Trans. Power Electron.*, vol. 33, no. 8, pp. 6957–6969, Aug. 2018, doi: 10.1109/TPEL.2017.2754324.
[18] K.-H. Kim, I.-C. Baik, G.-W. Moon, and M.-J. Youn, "A current control for a permanent magnet synchronous motor with a simple disturbance estimation scheme," *IEEE Trans. Control Syst. Technol.*, vol. 7, no. 5, pp. 630–633, Sep. 1999, doi: 10.1109/87.784427.
[19] C. Martin, M. R. Arahal, F. Barrero, and M. J. Duran, "Five-phase induction motor rotor current observer for finite control set model predictive control of stator current," *IEEE Trans. Ind. Electron.*, vol. 63, no. 7, pp. 4527–4538, Jul. 2016, doi: 10.1109/TIE.2016.2536578.
[20] Z. Song and F. Zhou, "Observer-based predictive vector-resonant current control of permanent magnet synchronous machines," *IEEE Trans. Power Electron.*, vol. 34, no. 6, pp. 5969–5980, Jun. 2019, doi: 10.1109/TPEL.2018.2870904.
[21] M. S. Rafaq, A. T. Nguyen, H. H. Choi, and J.-W. Jung, "A robust high-order disturbance observer design for SDRE-based suboptimal speed controller of interior PMSM drives," *IEEE Access*, vol. 7, pp. 165671–165683, 2019, doi: 10.1109/ACCESS.2019.2953073.
[22] J. Zhang, X. Liu, Y. Xia, Z. Zuo, and Y. Wang, "Disturbance observer-based integral sliding-mode control for systems with mismatched disturbances," *IEEE Trans. Ind. Electron.*, vol. 63, no. 11, pp. 7040–7048, Nov. 2016, doi: 10.1109/TIE.2016.2583999.
[23] X. Zhang, B. Hou, and Y. Mei, "Deadbeat predictive current control of permanent-magnet synchronous motors with stator current and disturbance observer," *IEEE Trans. Power Electron.*, vol. 32, no. 5, pp. 3818–3834, May 2017, doi: 10.1109/TPEL.2016.2592534.
[24] Y. Jiang, W. Xu, C. Mu, and Y. Liu, "Improved deadbeat predictive current control combined sliding mode strategy for PMSM drive system," *IEEE Trans. Veh. Technol.*, vol. 67, no. 1, pp. 251–263, Jan. 2018, doi: 10.1109/TVT.2017.2752778.
[25] J. Davila, L. Fridman, and A. Levant, "Second-order sliding-mode observer for mechanical systems," *IEEE Trans. Autom. Control*, vol. 50, no. 11, pp. 1785–1789, Nov. 2005, doi: 10.1109/TAC.2005.858636.
[26] R. Yang, M. Wang, L. Li, Y. Zenggu, and J. Jiang, "Integrated uncertainty/disturbance compensation with second-order sliding-mode observer for PMLSM-driven motion stage," *IEEE Trans. Power Electron.*, vol. 34, no. 3, pp. 2597–2607, Mar. 2019, doi: 10.1109/TPEL.2018.2845705.
[27] Y. Xu, X. Ding, J. Wang, and C. Wang, "Robust three-vector-based low-complexity model predictive current control with supertwisting-algorithm-based second-order sliding-mode observer for permanent magnet synchronous motor," *IET Power Electron.*, vol. 12, no. 11, pp. 2895–2903, Sep. 2019, doi: 10.1049/iet-pel.2018.5750.
[28] T. Gonzalez, J. A. Moreno and L. Fridman, "Variable gain super-twisting sliding mode control," *IEEE Trans. Autom. Control*, vol. 57, no. 8, pp. 2100–2105, Aug. 2012, doi: 10.1109/TAC.2011.2179878.

TIANXING LI was born in Shanxi, China, in 1990. He received the B.S. degree in electrical engineering from the Xi'an University of Technology, Xi'an, China, in 2012, and the M.S. degree from the School of Automation, Northwestern Polytechnical University, Xi'an, where he is currently pursuing the Ph.D. degree. His research interests include multiphase permanent-magnet electric machines drives, fault diagnosis, and fault-tolerant control.

RUIQING MA (Member, IEEE) received the B.S., M.S., and Ph.D. degrees from Northwestern Polytechnical University, Xi'an, China, in 1985, 1988, and 2007, respectively, all in electrical engineering. He is currently a Professor of electrical engineering and an Associate Director of the Institute of REPM Electrical Machines and Control Technology, Northwestern Polytechnical University. Since 1993, he has been teaching and conducting research on electric machines and power converters with Northwestern Polytechnical University. His research interests include rare-earth permanent-magnet electric machines drives, power converters, and renewable energy systems.

WEIJIAN HAN (Member, IEEE) received the B.S., M.S., and Ph.D. degrees from Northwestern Polytechnical University, Xi'an, China, in 2012, 2015, and 2019, respectively, all in electrical engineering. From 2016 to 2018, he was a Visiting Ph.D. Student with the Department of Information Engineering, University of Padova, Padova, Italy. He is currently a Lecturer with the State Key Laboratory of Reliability and Intelligence of Electrical Equipment, Hebei University of Technology. His research interests include modeling and digital control for bidirectional dc–dc converters and permanent magnetic motor drives.